Chapter 5
Graphene Oxides in Filtration and Separation Applications

Zhiping Xu

Abstract Graphene oxides feature much richer structural and physiochemical properties than the two-dimensional crystal graphene they are derived from. The stacked structures as well as functional groups and defects in the monatomic layers lead to a porous microstructure and engineerable channels for selective transport of water, ions, and gases across the graphene oxide membranes. Additional merits include their facile fabrication, low cost, and flexibility. Recent efforts in exploring the structure–property relationship of these materials and environment and energy-related applications not only demonstrate excellent balance between the permeability and selectivity of fluid transport through the graphene oxide membranes, but also deepen our understanding of the molecular transport mechanisms down to the nanoscale. In this chapter we review some of the major theoretical and experimental advances in this field, along with our perspectives for the future development.

Keywords Graphene oxides • Filtration • Separation • Microstructure • Permeation • Selectivity

5.1 Introduction to Molecular Filtration and Separation

Recent crisis of water resource shortage, especially in developing countries, has raised immersed research interests in new clean water technologies [1]. As illustrated in Fig. 5.1, membrane-based technologies such as ultrafiltration (UF), nanofiltration (NF), reverse osmosis (RO), and forward osmosis (FO) have received enormous attention because of their low cost and effective energy utilization for removing contaminants from water. These technologies have already been widely used in a broad spectrum of industries such as water purification and food processing. Designed for membrane-based water desalination and wastewater treatment applications, porous

Z. Xu (✉)
Applied Mechanics Laboratory, Department of Engineering Mechanics
and Center for Nano and Micro Mechanics, Tsinghua University, Beijing 100084, China
e-mail: xuzp@tsinghua.edu.cn

W. Gao (ed.), *Graphene Oxide*, DOI 10.1007/978-3-319-15500-5_5

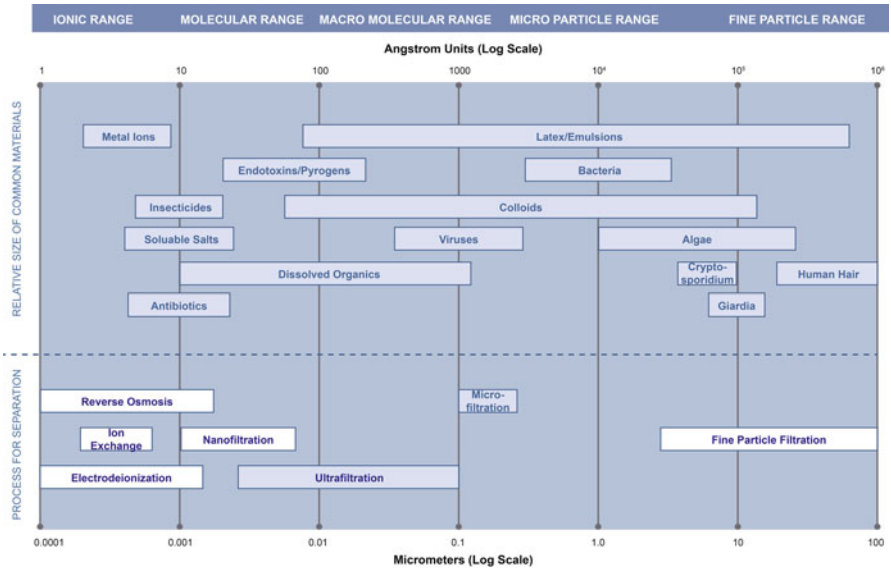

Fig. 5.1 Filtration and separation spectrum that shows characteristic length scales and mechanisms of the technologies

nanostructures with tubular or laminar topologies have been explored by conducting precise measurements in experiments and molecular level computer simulations [2–6]. Using porous structures with a dimension on the order of one nanometer that is close to the size of water molecules or ions, one could achieve high salt rejection in water desalination or high selectivity for ion separation. Moreover, researches have demonstrated unexpected high permeability of water through nanochannels due to the fact that the flow resistance is remarkably reduced under nanoscale constriction [7–9]. As a result, with an optimally designed architecture, nanostructured membranes could be scaled up for industrial applications with performance far beyond existing technologies.

Compared to conventional membrane materials such as the zeolites, porous silica, and polymers, the graphene oxide (GO) membrane with functionalized monatomic layers as building blocks is an ideal material for these applications. The rich chemistry of functional groups results in differentiation in the interaction between ions and GO. Its tunable microstructures and physiochemical properties thus allow rational design of selective fluidic transport at the molecular level, offering exciting opportunities in establishing high-performance and low-cost clean water technologies. GO membranes have also been considered as permeable membranes for selective gas transport. Their nanoporous microstructures and species-specified adsorption enable gas separation or capture based on the mechanisms of molecular sieving or adsorption. Promising applications could be found in the environmental and energy industry, e.g., CO_2 capture from flue gas, CO_2 removal from natural gases, CO_2 recovery from landfill gas, and selective hydrogen separation.

In the following part of this chapter, we first introduce the atomic structures of GO and microstructures of GO membranes in Sect. 5.2, and the mechanism of filtration and separation in Sect. 5.3. A few representative works in developing relevant applications that have been reported recently are reviewed in Sect. 5.4, followed by our concluding remarks and perspectives in Sect. 5.5.

5.2 Structures of GO and GO Membranes

As discussed previously in Chap. 1, the GO layer consists of oxygen-rich functional groups as well as vacancy-like defects within the sheet. The density and spatial distribution of these imperfections, as well as their modulation of the microstructures of GO membranes, define the strength of gas adsorption, resistance to molecular flow, and ionic affinity in various environments. From a design point of view, as the hydrophilicity and solubility of GO sheets allow them to be well dispersed in solution as single-layer sheets, their atomic structures could then be engineered before assembled into membranes. In this section we review briefly current understandings of the atomic and microscale structures of GO membranes, before continuing discussions on their implications in the separation and filtration processes.

5.2.1 Atomic Structures of Graphene Oxide

Models of graphene oxides: As a product of strong acid/base treatment, the atomic structure of GO is quite disordered compared to the hexagonal lattice of crystalline graphene. The single-layer sheet usually contains oxygen-rich functional groups such as hydroxyl and epoxide groups on the carbon basal plane, carboxyl, carbonyl, and phenol groups to the edges of sheets or nanoholes embedded, as well as lactol rings [10, 11]. A schematic illustration is shown in Fig. 5.2a. These functional groups are usually negatively charged and interact with molecules or ions with different strengths according to their atomic charges and polarization. The covalently bonded network in GO is defective after the oxidation-reduction treatment. Experimental evidence studies suggest the existence of defect-free graphene areas with size of a few nanometers interspersed with defect areas that are dominated by clustered pentagons and heptagons (Fig. 5.2b). All carbon atoms in the defective areas are bonded to three neighbors maintaining a planar sp^2 configuration with relative chemical stability. However, significant in-plane distortions and strain in the surrounding lattice as well as out-of-plane displacement are introduced [12]. Considering that interlayer gallery, interedge spaces, and embedded pores can be occupied by the fluid, both basal-plane and edge functionalization play important roles in determining the percolated paths for molecular transport, and thus the permeability and selectivity in separation and filtration applications (Fig. 5.2c).

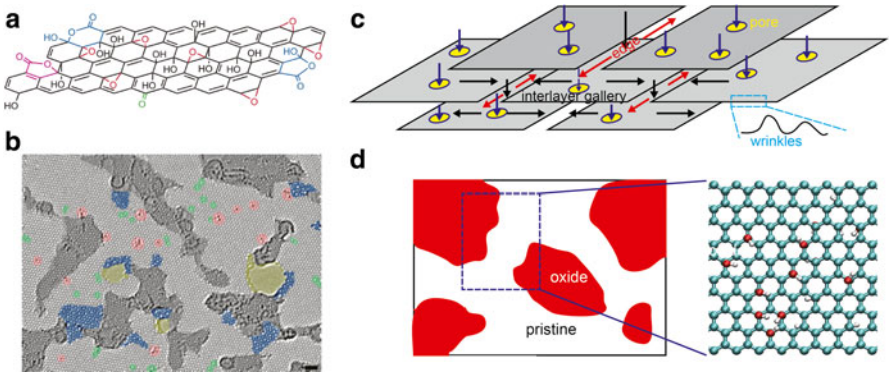

Fig 5.2 (**a**) Atomic structures of a single-layer GO sheet, taking into account the five- and six-membered lactol rings, ester of a tertiary alcohol, hydroxyl, epoxy, and ketone functionalities. The model here only shows the chemical connectivity, but not the steric orientation of these functionalities [11]. (**b**) Defective structures of GO characterized by the high-resolution transmission electron microscopy. The defect-free crystalline graphene area is displayed in *light-gray color*. Contaminated regions are shaded in *dark gray. Blue regions* are the disordered single-layer carbon networks, or extended topological defects, that are identified as remnants of the oxidation–reduction process. *Red areas* highlight individual ad-atoms or substitutions. *Green areas* indicate isolated topological defects, that is, single-bond rotations or dislocation cores. Holes and their edge reconstructions are colored in *yellow*. The scale bar is 1 nm [66]. (**c**) Illustrated microstructures of GO membranes that comprise stacked GO sheets. Paths opened for molecular transport consist of the interlayer gallery, slit-like interedge spacings, embedded pores, and channels formed by the wrinkles of GO sheets [5, 6]. (**d**) An atomistic model of GO constructed for atomistic simulations [5, 6]. (Reproduced by permission from NPG, ACS)

Clustering of functional groups: In addition to the type of functional groups and defects, their spatial distribution is also important in specifying the percolated path for molecular transport. Results from experimental characterization and computer simulations have been reported to support that the basal-plane imperfections tend to agglomerate and form clusters, leading to a patched nature of structural modification comprising both pristine and oxide regions, as well as nanoholes (Fig. 5.2d) [12–15]. As a result, a 2D percolated path along the unfunctionalized region could be formed in the interlayer gallery to enable fluidic transport with low wall friction.

Surface modification and interlayer intercalation: One of the most attractive features of GO is that the structure could be functionalized or modified before the isolated sheets are assembled into membranes. This process could be designed to tune the density and spatial distribution of functional groups, defects, the nanopores they induce, as well as the surface charge and lateral size of GO sheets [16–20]. The structure of GO membranes in liquid solvents is found to be quite dependent on the liquid molecules. While GO membranes are easily hydrated by water, intercalation of alcohols is hindered and the insertion of ethanol into the membrane is limited to only one monolayer [21]. For GO membranes in contact with solution or humid air, the interlayer gallery changes upon hydration. The negatively charged, highly hydrophilic surface of GO favors the intercalation of water molecules that could lead to the formation of

hydrogen bond (H-bond) networks [22]. The water contact angle of graphene $\theta_{c,G}$ is in the neutral range of 87–127°. However, after functionalization the water contact angle of GO $\theta_{c,GO}$ decreases with the concentration of oxygen-rich functional groups on the sheet. For a typical concentration of O:C = 20 % for GO, $\theta_{c,GO}$ is calculated to be 26.8° [23]. The hydrophilicity of GO allows the membrane to expand by intercalating water molecules. Experimental measurements show that the interlayer distance measured for bilayered GO increases by ~0.1 nm, from ~0.7 to 0.8 nm, when exposed in the environment with a relative humidity in the range of 2–80 %, while immersion into liquid water raises the value up to ~1.2 nm [24]. According to the patched nature of GO sheet, the functionalized regions act as spacers that keep adjacent crystallites apart, with tunable interlayer distance depending upon the humidity, and prevent them from being dissolved, whereas pristine regions provide a network of capillaries that allow low-friction molecular transport [5, 6, 25, 26]. In addition to water, GO sheets could also be engineered by other functionalization approaches such as ion and polymer intercalation, which control the size and charge characteristics of the transport channels in separation and filtration applications [27–29].

5.2.2 *Microstructures of Multilayer Graphene Oxide Membranes*

For the permeation and selectivity of a porous membrane, not only the physiochemical properties of pore surfaces are relevant, but also the structural characteristics are of great importance in defining the membrane performance, which can be quantified through the porosity p and tortuosity τ. The porosity is the relative volume of the membrane that could be occupied by the fluid, while the tortuosity is the ratio between the average length of the fluid paths and the geometrical length of the sample. The permeability measuring the ratio between the flow rate and pressure gradient could be enhanced by increasing the factor p/τ. The microstructures of GO membranes, although difficult to be resolved in detail experimentally, could be controlled during the fabrication process through, for example, the sheet size, functionalization level, as well as template-enabled controls.

Brick-and-mortar microstructures: As illustrated in Fig. 5.2c, the open network for fluid flow across the GO membrane consists of two major paths. The first one travels through the nanopores within GO sheets or the slit-like interedge spacings. Due to the random stacking order during the synthesis, the alignment between these structures embedded in the neighboring layers of the brick-and-mortar structure will only be possible for ultrathin membranes [30]. As the thickness increases, the species in transport must flow through the interlayer gallery before they find a pore or slit to go through. This additional cost in general reduces the flow rate and becomes the rate-limiting process of the cross-membrane flow. The second path for molecular flow is within the interlayer gallery, along the most efficient channels that could be the pristine graphene regions with less resistance against the flow or the wrinkles and nanochannels as we discuss below [25, 31, 32].

Corresponding to these two regimes of molecular transport, two types of membrane could be designed for filtration and separation applications, where the fluid flow is driven across or along the GO sheets. In either case, enlarging the interlayer distance by molecular intercalation or other spacers, increasing the in-plane defects by exotic treatments such as heating, irradiation, or chemical functionalization, or choosing GO sheets with smaller lateral sizes in the fabrication could improve their permeability, although it should be kept in mind that the selectivity and mechanical resistance of membrane could be sacrificed with these modifications.

Wrinkles: As a 2D material, the long-range crystalline disorder of graphene could not be maintained in a freestanding manner. Out-of-plane corrugations induced by thermal fluctuation of the presence of defects within the GO sheets become prominent even when they are constrained, unless the graphene or GO sheets are very strongly adhered to a substrate or inside a matrix. The athermal fluctuation of 2D sheets is an intrinsic feature of GO as a defective monatomic layer, arising from the formation of sp^3 hybridized atomic structures and topological defects such as non-hexagonal rings. The local structural corrugation thus induced is on the order of one nanometer [12]. These defects and thermal fluctuation are also expected to affect the overall morphology of the sheet and the long-range correlation can hardly be preserved during the membrane synthesis process. The functional groups on GO could roughen the potential surface that describes the interaction between neighboring GO sheets, leading to local stacking structures that lock channel-like structures in between [33]. These microstructural corrugations can become part of the transport channel network in the membrane and could be altered in the solvated and dry conditions as the capillary forces occurring during the drying process could flatten the GO sheets [34]. Tuning the synthesis and fabrication processes of GO is demonstrated to be able to control the microstructures of GO membrane. For example, by changing the temperature of hydrothermal reduction process from 90 to 150 °C, the effective pore size for nanoparticle rejection increases from 3 to 13 nm, which is mainly attributed to the wrinkled membrane structures. Further experimental evidences from direct yellow nanofiltration tests suggest that this control of corrugation could even reach the scale of sub-nanometer [31].

Nanochannels: Microstructures of GO membranes could also be rationally engineered to enable or enhance their functions. For example, nanostrand-templated GO membranes display excellent ultrafiltration performance (Fig. 5.3). A network of nanochannels with a narrow-size distribution between 3 and 5 nm is created in the membrane that offers superior separation performance. The permeance shows a tenfold enhancement without sacrificing the rejection rate compared with that of common GO membranes, and is more than 100 times higher than that of commercial ultrafiltration membranes with similar rejection. With a viscous nature of flow, the enhancement is attributed to the enriched porous structures by nanochannels that significantly reduces the overall channel length and enhances the p/τ ratio. Moreover, an abnormal pressure-dependent separation behavior is identified as the nanochannels could deform reversibly, leading to modulations in the water flux and rejection rate. As a result, the membrane performance can be tuned through pressure control, enabling promising mechanomutable applications.

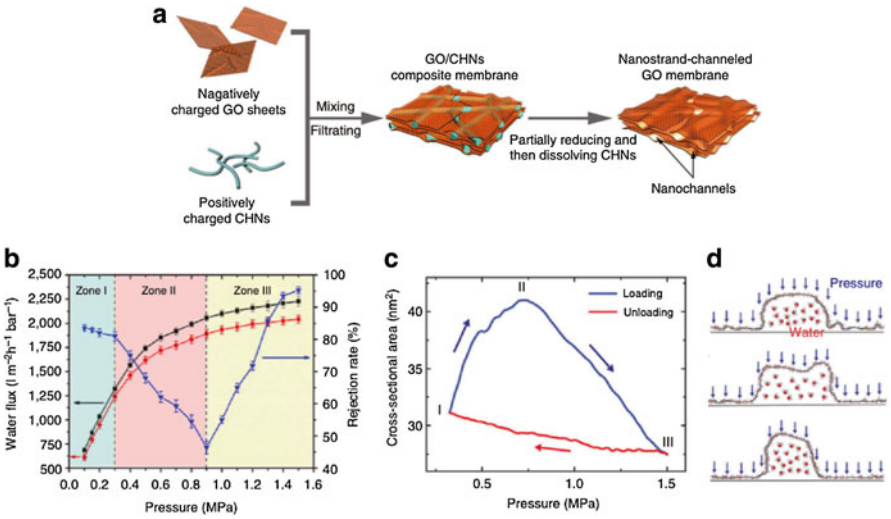

Fig. 5.3 (**a**) Illustration of the multistep fabrication process of nanostrand-channeled GO membrane, consisting of the formation of a dispersion of positively charged copper hydroxide nanostrands (CHNs) and negatively charged GO sheets on a porous support, followed by hydrazine reduction, and finally nanostrand removal. (**b**) Pressure-dependent flux and rejection of Evans blue molecules of the membrane. The *black squares* and *red circles* represent the water flux during the first and third pressure-loading cycles, respectively. The *blue triangles* denote the rejection rate within the first cycle. (**c**) Simulated changes in the cross-sectional area of nanochannel as a function of the applied pressure. (**d**) The response in deformation of a GO nanochannel under pressure loading, modeled in molecular dynamics simulations. The amplitude of applied pressure increases from top to the bottom. The cross section of nanochannels is flattened first with a larger area and then compressed at higher pressure [32]. (Reproduced by permission from NPG)

5.3 Mechanisms of Selective Molecular Transport in Graphene Oxide Membranes

Membrane filtration is usually understood as a dynamic process where fluid dynamics and electrochemistry govern. However, down to the nanometer scale, the conventional theories need to be updated, if not changed, to describe and predict new phenomena in related applications [5, 6, 18–20, 25, 35, 36]. The brick-and-mortar hierarchy of GO membrane allows both cross and in-plane flow of molecules. The first process relies on the presence of vacancy-like defects in GO or slit-like interedge spaces between neighboring GO sheets aligned in plane. Although in cross flow, molecular transport directly across the GO sheets travels much shorter distance than the in-plane flow between neighboring GO layers, its participation is only significant in ultrathin membranes that consist few GO layers, for example, considering GO membranes with defects or slit-like interedge spacings with widths of w and areal densities of n. The probability to find a straight path across an N-layer membrane then decreases drastically as $2(wn)^{N-1}$ [5, 6]. To enhance the cross-flow

permeability, one must increase either the size of pores in GO or their concentration, which will, however, reduce the selectivity and mechanical resistance as a cost. Otherwise, molecular transport within the interlayer spacings is unavoidable and the whole transport network will include both the interlayer gallery and nanopores inside the GO sheet. As a result, confined molecular transport through these nanoporous structures becomes the key to understand the filtration process.

5.3.1 Selective Transport of Liquid and Gas

Viscous flow with slip boundary conditions: Confined viscous flow such as flow inside a pipe or between parallel plates could be captured using the Navier–Stokes equation in the continuum regime. A non-slip boundary condition is commonly assumed in exploring viscous flow at macroscale, where the flow velocity decreases to zero at the wall surface. However, within nanoscale channels, the atomic structures of fluid tend to deviate from the bulk. Atomistic simulation results show that the intercalated water between GO sheets displays layered structures, from

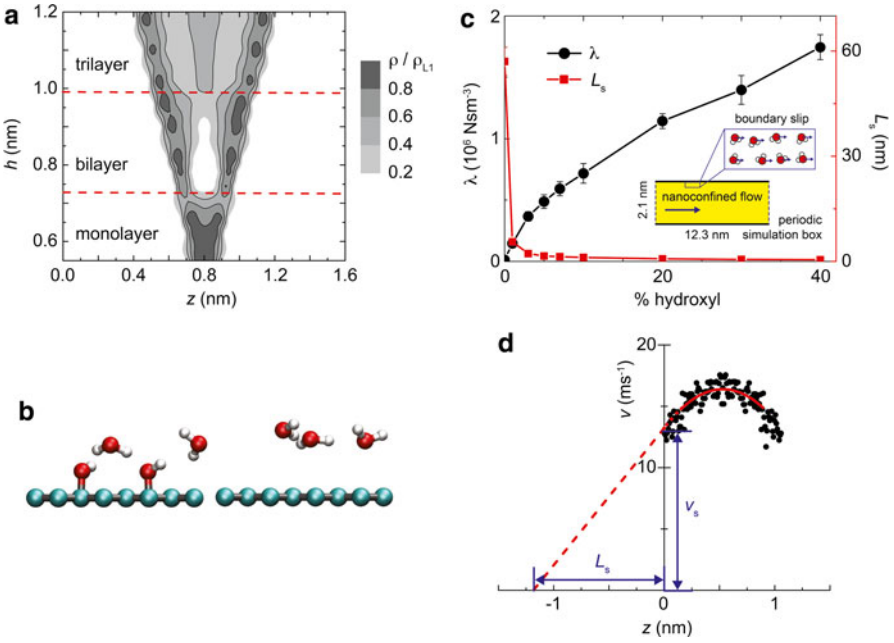

Fig. 5.4 (**a**) Density profiles of water molecules intercalated between GO sheets, which shows the transition from single layer, bilayer, and trilayer to more disordered structures as the interlayer distance increases. (**b**) Atomistic simulation snapshots that show water molecules in the first water layer at the GO (*left*) and graphene (*right*) wall. The distances between the water molecules and the basal planes are close in these two different structures. (**c**) The dependence of frictional coefficient and interfacial slip length on the concentration of hydroxyl groups functionalized on GO. (**d**) The velocity profile of water flow between GO sheets and the definition of slip length [5, 6]. (Reproduced by permission from APS)

monolayer, bilayer, to trilayer with the interlayer distance below 1.2 nm as illustrated in Fig. 5.4a [5, 6]. Interestingly, although the GO sheet contains surface functional groups, the distance between the first water layer and the basal plane in GO remains the same as that between graphene sheets at the interlayer distance (Fig. 5.4b). As a result, the interlayer gallery in GO membrane is actually a 2D planar channel containing layered water content, with uniform thickness but heterogeneous surface properties if the wrinkles are not considered.

Water transport in nanoscale channels has received much interest recently from both fundamental research and practical applications. Research has shown that the combined effect from nanoconfinement and atomistically smooth graphitic walls leads to significant flow enhancement inside carbon nanotubes (CNTs) or between graphene sheets, in comparison to theoretical predictions from the Navier–Stokes equation supplied with non-slip boundary conditions. The flow enhancement could be quantified through the definition of Navier slip length $L_s = v_s/(\mathrm{d}v/\mathrm{d}z)|_{z=0}$, where v_s is the slip velocity at the fluid-wall interface and $\mathrm{d}v/\mathrm{d}z$ is the tangent of the velocity profile along the normal direction z at the wall ($z=0$) (Fig. 5.4c, d). Experimental studies have revealed that for CNTs with an inner pore size of a few nanometers, a slip length over micrometers could be established [37–39]. Although the reported values of L_s have some discrepancy due to the differences in experimental samples, conditions of measurements, or theoretical models, the large boundary slip that elevates the overall flow rate clearly demonstrates the advantage of using nanostructured materials in environmental applications.

Graphene, considered as the zero-curvature limit of the CNT, can also form nanoscale flow channels while stacked into multilayers. However, the van der Waals cohesion between pristine graphene sheets results in an interlayer distance of 0.34 nm that cannot accommodate even a single water molecule. Functionalized graphene sheets, such as GO and polymer-intercalated graphene sheets, offer a wider interlayer space for molecular transport, and the size can be further tuned by engineering the structure or environmental conditions. For non-slip planar flow between GO sheets, the volumetric flux Q can be estimated as $Q_{\mathrm{nonslip}} = -\mathrm{d}^3 \Delta PW/(12\eta L)$, where d is the channel thickness that should be redefined here as the hydrodynamic thickness by excluding the vacuum space $\delta = 0.5$ nm between water molecules and the carbon basal plane. However, once the boundary slip is considered through the slip length L_s, the flow rate could be enhanced by a factor of $\varepsilon = Q_{\mathrm{slip}}/Q_{\mathrm{nonslip}} = 1 + 6L_s/d$, which is significant if the atomistic smoothness of the wall is well preserved and a large slip length of micrometers is available.

Once the atomistic smoothness is broken by the presence of functional groups as in the situation of GO, the flow enhancement is weakened remarkably. Studies using atomistic simulations show that the enhancement factor could be reduced by two orders, from 48.13 to 0.44 nm for a typical concentration of oxidization groups with O:C = 30 %. That is to say, even with the nanoconfinement, the water flow between GO layers is viscous and the flow rate should be estimated using non-slip boundary conditions [5, 6, 32, 40].

It should be noted that there are some evidences showing that the oxidization of GO sheets is not spatially uniform. Functional groups could group into clustered patterns and leave flow paths comprising pristine graphene channels in the GO membrane. A fast lane for water transport may exist based on the fact that water flow over graphene sheet

experiences ultralow friction [25, 41]. However, the oxidized region of GO is also wetted with negligible boundary slip for the flow. Even if a percolated path could be formed along the pristine region of GO, the internal friction between water molecules in the pristine and oxidized regions at their interface could impede flow within the pristine paths. This side-pinning effect can only be neglected if the width of pristine channels is much larger than the size of 1–2 nm that is characterized in experiments [5, 6].

Water transport through nanopores or interedge spaces inside GO was also explored by molecular dynamics simulations, which suggest that the permeability is close to that of flow between GO sheets, but is significantly reduced compared to that between pristine graphene sheets with the same channel width. To estimate the overall permeability across the GO membrane in practical situation, the entrance/exit loss and capillary-driven force must also be considered [25, 42].

Gas permeation: Similar to the mass transport of liquid molecules, selective gas permeation through GO membranes could also be established by balancing the performance trade-off between mobility of gas molecules and the selectivity, which could be enabled by either the molecular size-sieving mechanism or the difference in gas adsorption and diffusion behaviors. For gas transport confined by nanoscale pores, the flow regime changes from Knudsen diffusion for mesopores from 2 to 50 nm to constrained molecular diffusion for micropores below 2 nm. The Knudsen flow model fits the situation where the mean free path of gas molecules is longer than the size of pores, where diffusion is limited by thermalized collisions with the wall. Based on this assumption, the permeability could be estimated as $pd/3\tau h(8/\pi m\mathrm{R}T)^{1/2}$, where d is the pore size, m is the molecular weight, R is the ideal gas constant, and T is the temperature. Thus the separation of gases could be achieved through differentiating the molecular weight [16, 35].

For the constrained diffusion of gases, the gas permeation is dominantly determined by their interaction with the pore wall and their kinetic diameters. One way to quantify these effects is through the self- and collective or transport diffusivities [43]. Similarly, rapid transport of gases in carbon nanotubes with pristine graphitic walls was reported, which are orders of magnitude faster than in the zeolites with comparable pore sizes [35, 44]. However, in corrugated GO membranes with negatively charged functional groups on the surfaces, the gas permeability would be significantly reduced to the flow between graphene sheets with the same interlayer distance. Moreover, in addition to the selectivity based on molecular weights or kinetic diameters of the gases, interaction with the wall adds another dimension in establishing the separation of polar molecules such as CO_2.

5.3.2 Selective Ion Transport

One of the major targets of water desalination, recovery, and recycling processes is to selectively remove ions from the water. The ionic selectivity is defined by the size, shape of ions, as well as their interaction with the hydrophilic, negatively charged GO membrane. In aqueous form, ions are gel-like by possessing

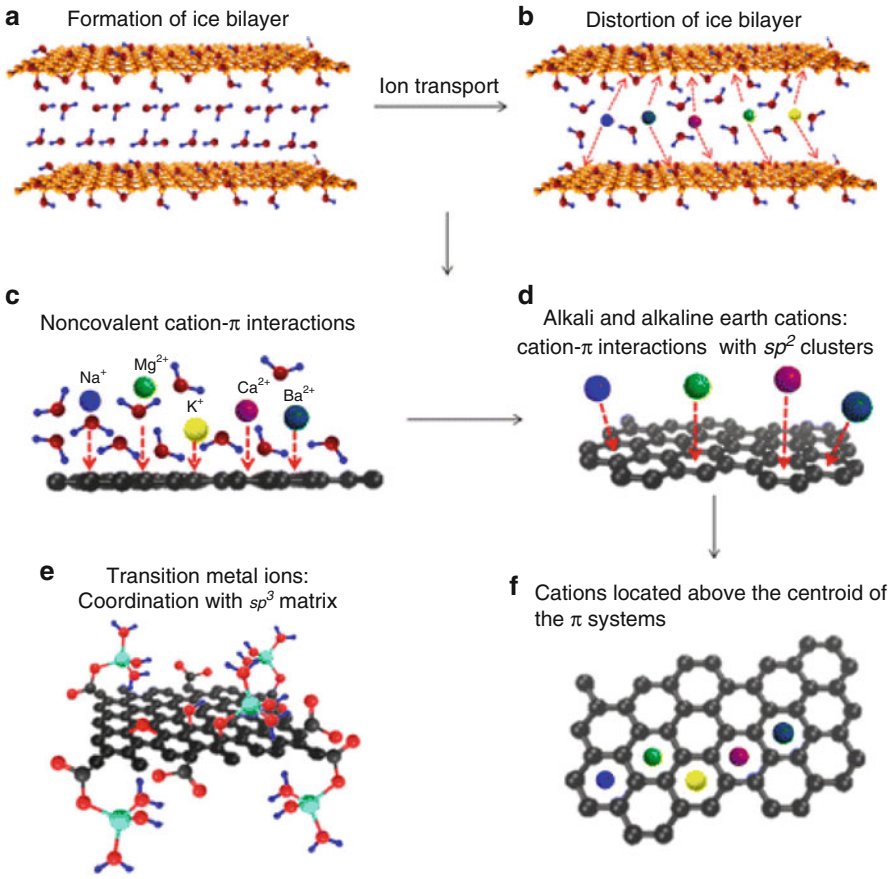

Fig. 5.5 Schematic diagrams of selective ion transport through GO membranes and the diverse interactions between different cations and GO [18–20]. (Reproduced by permission from ACS)

surrounding hydration shells of water molecules. The strength of hydration depends on the type of ions. For example, small monovalent ions (Li^+, Na^+, F^-) feature much stronger hydration energy than larger ones (K^+, Cl^-, Br^-, I^-). The ions possessing higher charge densities also bind stronger with larger water clusters. Moreover, the anions hold their hydration shells relatively more strongly than the cations due to the difference in the strength of ion-water interaction [45] (Fig. 5.5).

For ions confined between nanochannels with pore sizes comparable to those of the hydrated ions, such as those that conduct across the GO membranes, the solvation shell could be strongly disturbed. Considering the similarity between negatively charged oxygen-rich groups on the GO surface and polar water molecules, the mechanisms of ionic permeation and selection become more complicated than the simple picture of molecular sieving. Firstly, the interaction between GO and the ions could then differ by the level of ion hydration, and the oxygen-rich groups could behave as part of the solvation shell. At the same interlayer distance, electrostatic interaction

between GO and small ions could be better screened and the permeation rate could then be higher [18–20]. Secondly, as the width of nanochannels becomes comparable or smaller than the Debye screening length, the interaction between the oxygen-rich groups on GO and conducting species starts to play an important role. As both pristine and oxidized regions coexist in the GO membrane, not only their coordination with transition metal ions but also the cation–π interaction between the graphitic regions and main-group cations are responsible for the selective ion transport in addition of sieving the solvated ions by their sizes [18–20, 36, 40].

5.4 Recent Progresses in the Experimental Demonstrations Towards Applications

With the capabilities of measuring the water and ion permeance, selectivity, as well as characterizing the microstructures of GO membranes, significant efforts have been made recently to understand the underlying mechanisms of selective liquid and gas transport, and explore their potential applications in the filtration and separation applications. The proposed mechanisms introduced in the previous section are justified based on evidences from experimental and computational studies, to upgrade the current understandings of the ultimate design of membranes for filtration and separation by engineering single-atom-thick 2D materials.

5.4.1 Water Purification

Submicrometer-thick GO membranes were reported to be completely impermeable to liquids, vapors, and gases including He, but allow unimpeded permeation of water, which is at least 10^{10} times faster than He [25]. The measurements were done by analyzing the evaporation rates of species across GO membranes from their weight loss. Impressively, the unimpeded water permeation in submicrometer GO membranes is as fast as water evaporation through an open aperture, suggesting an evaporation-limited regime. The fast water permeation through the membrane is explained as the presence of a high capillary pressure formed between GO sheets, and a large, percolated path of pristine, unoxidized graphene regions that allow water flow with ultralow friction. Moreover, compared to the as-prepared GO, the interlayer distance in reduced GO by thermal annealing decreases significantly from ~1 to ~0.4 nm. As a result, the water permeability is reduced remarkably by 100 times, which indicates the significance of in-plane transport within the interlayer gallery and the critical role of interlayer distance in the molecular sieving process.

Reduced GO membranes with a thickness of 22–53 nm were fabricated on a microporous substrate for use in nanofiltration-based water purification [30]. These ultrathin membranes demonstrate high pure water flux of 21.8 $Lm^{-2}\ h^{-1}\ bar^{-1}$, high retention for organic dyes >99 %, and moderate retention of ~20–60 % for ion salts. Both physical sieving and electrostatic interaction between the charged groups in GO the rejection

process and analysis of the flow rate suggest the possibilities of water flow through nanopores and slits within the GO layers. It is further shown that as the membrane thickness increases from 22 to 53 nm, the pure water flux across the membrane decreases dramatically from 21.8 to 3.26 $Lm^{-2}\ h^{-1}\ bar^{-1}$. Moreover, the retention measured for different salt solutions agrees with theoretical predictions from the Donnan exclusion theory, which links the salt retention to the valences of cationic and anionic species.

5.4.2 Ion Separation

Ion transport through GO membranes was investigated using a nanofluidic device [46]. The massive parallel 2D channels between neighboring GO layers are percolated that allow efficient in-plane ionic transport. The ionic conductance measured is as high as that of the bulk electrolyte solution at high salt concentration. However, at low salt concentration below ~0.05 M, the conductance deviates from bulk behavior and displays a concentration-independent, surface-charge-governed regime of ionic transport (Fig. 5.6a–d). The negatively charged nature of GO also leads to high affinity to the cations while anions are repelled, allowing ion separation. The flexibility of the GO paper-based nanofluid device was also demonstrated by mechanical folding for 30 cycles.

There are also experimental evidences showing that the hydrated radius of salt ions in a molecular sieving regime determines the rate of ion permeation [26]. The ions with sizes below the critical mesh size of the nanochannel permeate at almost the same rate, whereas large ions and organic molecules exhibit no detectable permeation (Fig. 5.6e). These results suggest that, to avoid ionic conduction, the size of interlayer channel should be controlled down at ~0.6 nm to allow monolayer water

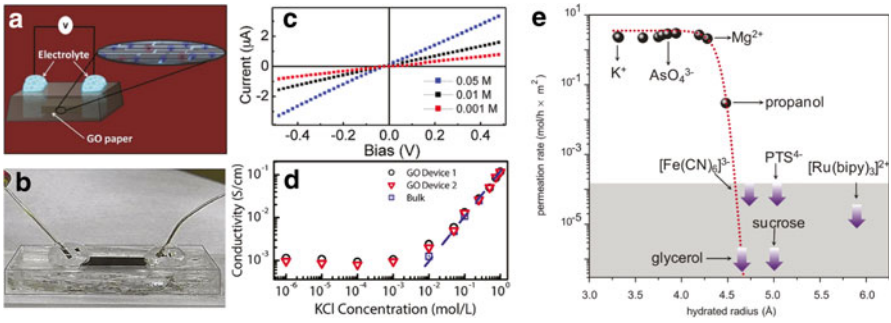

Fig. 5.6 (**a**) Schematic illustration and (**b**) photograph showing GO paper-based nanofluidics device. (**c**) Representative *I–V* curves recorded at different KCl concentrations. (**d**) Ionic conductivity as a function of salt concentration measured through GO nanochannels [46]. (**e**) Ionic permeation rates measured by using 5-μm-thick GO membranes. The *thick arrows* are detection limit in the measurements, and the *dashed curve* is a guide to the eye, showing an exponentially sharp cutoff at 0.45 nm with a width of ~0.01 nm [26]. (Reproduced by permission from ACS, AAAS)

transport and reject even the smallest salts. Nanopores or interedge slits inside GO are expected to have the same critical size for ionic transport. However, a recent work shows that, as the extreme case of ionic transport, thermal protons are able to permeate through even perfect graphene lattice with a surprisingly low resistivity of 10^{-3} Ωcm^2 above 250 °C. The transport can be further enhanced by decorating the graphene monolayer with catalytic metal nanoparticles that could lower the tunnel barrier [47].

Selective ion permeation across GO membranes was studied by considering a wide spectrum of ion types. It was reported that sodium ions permeate much faster than heavy-metal salts such as Mn^{2+}, Cd^{2+}, and Cu^{2+}. Notably, copper sulfate and rhodamin B are blocked entirely because of their strong interactions with GO [36, 40, 48]. Specifically, the transition metal ions could be coordinated by the oxygen-rich groups on GO and thus be strongly impeded. Further investigation on alkali and alkaline earth cations shows relative transport rates in the order of $H^+ > Mg^{2+} > Na^+ > Ba^{2+}$, Ca^{2+}, and K^+, from the highest value to the lowest ones, which can be explained by a combined effect of π-cation interaction and nanoconfined hydration [18–20]. The permeability increases as the lateral size of GO sheet is reduced, where a shorter path is available for the ionic conduction. Moreover, a remarkable temperature dependence is observed from 20 to 40 °C. The ion penetrations increase significantly with temperature, indicating the role of thermal activation in the permeation. The ion transport through GO membrane is further demonstrated to be controllable under electromagnetic fields. Specifically, electric field can either increase or decrease the ion transport depending on the flow direction, while magnetic field can enhance the ion penetration monotonically [18–20] (Fig. 5.7).

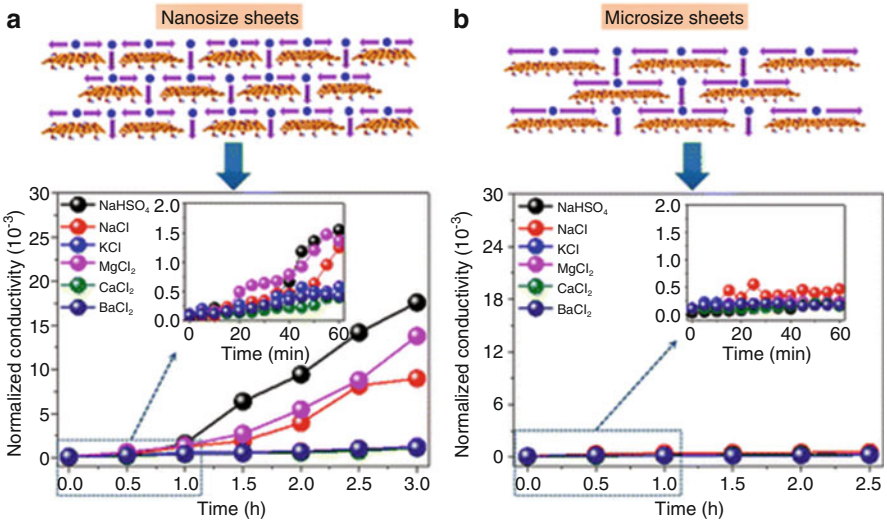

Fig. 5.7 Schematics of the lamellar structures and conductivities of cations across GO membranes composed of (**a**) nanosized and (**b**) microsized GO sheets. *Insets* show the initial stage (0–60 min) measurements of the penetrations [18–20]. (Reproduced by permission from ACS)

5.4.3 Gas Separation

A few experimental researches have been reported recently to explore selective gas transport across graphene (with in-plane defects generated during the growth and transferring processes) and GO membranes. Few and several layered membranes were engineered to exhibit excellent gas separation characteristics (Fig. 5.8). The close-packed, interlocked GO layered structures display an explicit effect on the selective gas transport. At 298 K, the order of gas permeability is $CO_2 > H_2 > He > CH_4 > O_2 > N_2$. The gas transport is determined by the pore size and the molecular mean free path in a gas mixture, and as in the Knudsen diffusion regime, gases are separated based on their differences in the molecular weight. The observed CO_2-philic behavior of permeation can be further enhanced by the presence of water, and high CO_2/N_2 selectivity can be achieved by well-interlocked GO membranes in a high relative humidity. More in-plane porous structures could be created by heat treatment, which leads to more permeable selective performance [16].

Gas-separation GO membranes down to 1.8 nm in thickness show H_2/CO_2 and H_2/N_2 selectivities of mixture separation that are one to two orders of magnitude higher than those of the state-of-the-art microporous membranes. The measured permeability is related to the kinetic diameter of gas molecules. Hydrogen molecules with a kinetic diameter of 0.289 nm permeate ~300 times faster than CO_2 (0.33 nm) through an 18-nm-thick GO membrane at 20 °C. The slight difference between their kinetic diameters suggests that a critical mesh size of the pore is ~0.289–0.33 nm. O_2 and N_2 show similar permeability as CO_2, while CO and CH_4 have slightly higher permeability although their kinetic diameters are larger. The membrane shows mixture

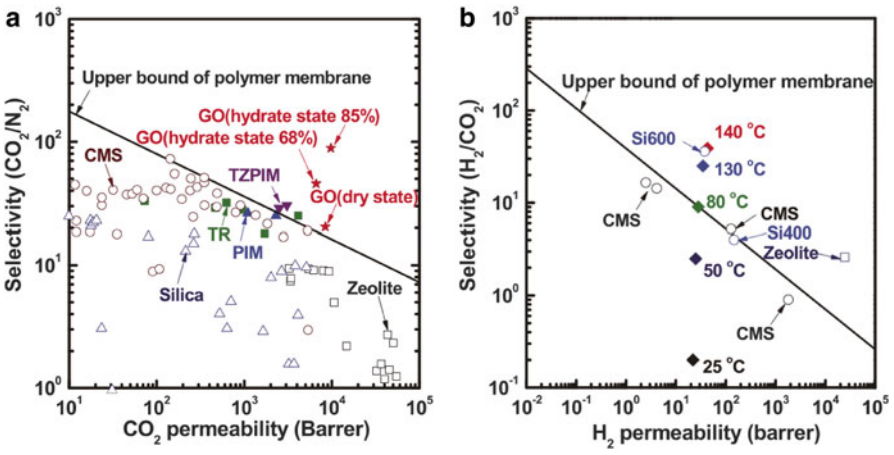

Fig. 5.8 (**a**) Relation between CO_2 permeability and CO_2/N_2 selectivity of GO membranes under dry and humidified conditions. (**b**) Comparison of gas separation performance between GO membranes and other membranes for the H_2 permeability and H_2/CO_2 selectivity [16]. (Reproduced by permission from AAAS)

separation selectivities as high as 3,400 and 900 for H_2/O_2 and H_2/N_2 through structural defects in GO, which are one to two orders of magnitude higher than those of the state-of-the-art microporous membranes. Moreover, the gas permeabilities decrease exponentially on the membrane thickness, which arises from the changes in the length of molecular transport paths [49].

Another detailed study shows that the intercalation of gas molecules is highly affected by the affinity between hydrophilic surface of GO and target molecules including CO_2, CH_4, H_2, and N_2. Only CO_2 can be intercalated into the GO membrane. However, the swelling of interlayer spaces in water changes the intercalation phenomena significantly. All of the tested gases could then be intercalated, but the CO_2 could be mostly solvated, surrounded by the intercalated water molecules and partially with functional groups on GO surfaces. Moreover, because the interaction between the intercalated water and GO retards the dynamics of water molecules, enhanced gas storage could be achieved within the intercalated water [50].

5.5 Conclusive Remarks and Perspectives

The understanding of nanoscale molecular transport mechanisms is of key importance to develop high-performance filtration and separation membranes. However, the current status is far from being mature. For transport through GO membranes, quantitative comparison between theoretical predictions and experimental measurements can hardly be made without detailed information of the microstructures. For example, the length of water transport channel can only be estimated very roughly based on the membrane thickness and average interlayer distance between neighboring GO sheets [25, 30, 32, 40]. To solve this issue, single-channel measurements should be carried out [51, 52], or the membrane fabricated should have a well-defined stacking order, uniform distribution of sheet size, shape, and functionalization of the GO sheets. Computational studies provide some insights into the process [5, 6], but the practical situation could be much different and complicated due to factors including the pH, salt concentration, pressure, thermal fluctuation, and electromagnetic fields, to list a few, which are difficult to be considered through atomistic models and are more appropriate to be explored experimentally [18–20, 53, 54].

Although impressive performance of GO membranes has been demonstrated by lab tests, there is still a gap existing towards their commercial utilization in industrial filtration and separation. To this end, large-scale fabrication of GO membranes that can maintain their structural stability in harsh environment should be established. Swelling of the GO laminates in solution should be avoided by mechanical constraints or chemical binding [26]. The mechanical resistance of GO to applied pressure is much weaker compared to the pristine graphene due to the presence of defects and surface functional groups, which should be assured especially for ultrathin membranes that are preferred for high permeance [55–57]. GO membranes could also be used as coating or barrier materials in related applications, where the supporting porous materials could provide the required structural stability [16, 49,

58]. However, the support layer could significantly weaken the performance of GO membranes for reasons such as the internal concentration polarization (ICP), which inevitably occurs inside the support layer and leads to a dramatic decrease in membrane flux and rejection rate. As a result, free-suspended GO membranes with desired mechanical resistance are highly demanded for industrial applications [59]. Moreover, the oxygen-rich groups could absorb either polar molecules or charged ions, resulting in significant amount of deposited residuals, which could break down the membrane performance and should be removed for regeneration.

There are also promising opportunities along the direction of membrane development using 2D materials, which can be considered as the ultimate material design due to the fact that all the atoms in these materials are exposed to the environment for engineering and the atomic structure could be tailored by a broad class of techniques. Efforts have already been made by considering other monolayer materials such as MoS_2 and graphyne [40, 60–63]. The molecular transport process through open channels in these materials could also be coupled with other functional processes such as electricity generation and energy harvesting [18–20, 52, 64]. Understandings of these functional processes could also inspire studies on transport and energetic processes in biological systems [65].

References

1. Shannon MA, Bohn PW et al (2008) Science and technology for water purification in the coming decades. Nature 452(7185):301–310
2. Kalra A, Garde S et al (2003) Osmotic water transport through carbon nanotube membranes. Proc Natl Acad Sci USA 100(18):10175–10180
3. Raghunathan AV, Aluru NR (2006) Molecular understanding of osmosis in semipermeable membranes. Phys Rev Lett 97(2):024501
4. Cohen-Tanugi D, Grossman JC (2012) Water desalination across nanoporous graphene. Nano Lett 12(7):3602–3608
5. Wei N, Peng X et al (2014) Breakdown of fast water transport in graphene oxides. Phys Rev E 89(1):012113
6. Wei N, Peng X et al (2014) Understanding water permeation in graphene oxide membranes. ACS Appl Mater Interfaces 6(8):5877–5883
7. Joseph S, Aluru NR (2008) Why are carbon nanotubes fast transporters of water? Nano Lett 8(2):452–458
8. Thomas JA, McGaughey AJH (2008) Reassessing fast water transport through carbon nanotubes. Nano Lett 8(9):2788–2793
9. Falk K, Sedlmeier F et al (2010) Molecular origin of fast water transport in carbon nanotube membranes: superlubricity versus curvature dependent friction. Nano Lett 10(10):4067–4073
10. Lerf A, He H et al (1998) Structure of graphite oxide revisited. J Phys Chem B 102(23): 4477–4482
11. Gao W, Alemany LB et al (2009) New insights into the structure and reduction of graphite oxide. Nat Chem 1(5):403–408
12. Gómez-Navarro C, Weitz RT et al (2007) Electronic transport properties of individual chemically reduced graphene oxide sheets. Nano Lett 7(11):3499–3503
13. Kim S, Zhou S et al (2012) Room-temperature metastability of multilayer graphene oxide films. Nat Mater 11(6):544–549

14. Kumar PV, Bardhan NM et al (2013) Scalable enhancement of graphene oxide properties by thermally driven phase transformation. Nat Chem 6(2):151–158
15. Zhou S, Bongiorno A (2013) Origin of the chemical and kinetic stability of graphene oxide. Sci Rep 3:2484
16. Kim HW, Yoon HW et al (2013) Selective gas transport through few-layered graphene and graphene oxide membranes. Science 342(6154):91–95
17. Andrikopoulos KS, Bounos G et al (2014) The effect of thermal reduction on the water vapor permeation in graphene oxide membranes. Adv Mater Interf 1(8):1400250
18. Sun P, Zheng F et al (2014) Electro- and magneto-modulated ion transport through graphene oxide membranes. Sci Rep 4:6798
19. Sun P, Zheng F et al (2014) Selective trans-membrane transport of alkali and alkaline earth cations through graphene oxide membranes based on cation–π interactions. ACS Nano 8(1):850–859
20. Sun P, Zheng F et al (2014) Realizing synchronous energy harvesting and ion separation with graphene oxide membranes. Sci Rep 4:5528
21. Talyzin AV, Hausmaninger T et al (2014) The structure of graphene oxide membranes in liquid water, ethanol and water-ethanol mixtures. Nanoscale 6(1):272–281
22. Compton OC, Cranford SW et al (2011) Tuning the mechanical properties of graphene oxide paper and its associated polymer nanocomposites by controlling cooperative intersheet hydrogen bonding. ACS Nano 6(3):2008–2019
23. Wei N, Lv C et al (2014) Wetting of graphene oxide: a molecular dynamics study. Langmuir 30(12):3572–3578
24. Rezania B, Severin N et al (2014) Hydration of bilayered graphene oxide. Nano Lett 14(7): 3993–3998
25. Nair RR, Wu HA et al (2012) Unimpeded permeation of water through helium-leak-tight graphene-based membranes. Science 335(6067):442–444
26. Joshi RK, Carbone P et al (2014) Precise and ultrafast molecular sieving through graphene oxide membranes. Science 343(6172):752–754
27. Park S, Lee K-S et al (2008) Graphene oxide papers modified by divalent ions: enhancing mechanical properties via chemical cross-linking. ACS Nano 2(3):572–578
28. Gao Y, Liu L-Q et al (2011) The effect of interlayer adhesion on the mechanical behaviors of macroscopic graphene oxide papers. ACS Nano 5(3):2134–2141
29. Hu M, Mi B (2013) Enabling graphene oxide nanosheets as water separation membranes. Environ Sci Technol 47(8):3715–3723
30. Han Y, Xu Z et al (2013) Ultrathin graphene nanofiltration membrane for water purification. Adv Funct Mater 23(29):3693–3700
31. Qiu L, Zhang X et al (2011) Controllable corrugation of chemically converted graphene sheets in water and potential application for nanofiltration. Chem Commun 47(20):5810–5812
32. Huang H, Song Z et al (2013) Ultrafast viscous water flow through nanostrand-channelled graphene oxide membranes. Nat Commun 4:3979
33. Xu Z, Buehler MJ (2010) Geometry controls conformation of graphene sheets: membranes, ribbons, and scrolls. ACS Nano 4(7):3869–3876
34. Zhang X, Wang Y et al (2011) Evaporation-induced flattening and self-assembly of chemically converted graphene on a solid surface. Soft Matter 7(19):8745–8748
35. Verweij H, Schillo MC et al (2007) Fast mass transport through carbon nanotube membranes. Small 3(12):1996–2004
36. Sun P, Zhu M et al (2013) Selective ion penetration of graphene oxide membranes. ACS Nano 7(1):428–437
37. Majumder M, Chopra N et al (2005) Nanoscale hydrodynamics: enhanced flow in carbon nanotubes. Nature 438(7064):44
38. Holt JK, Park HG et al (2006) Fast mass transport through sub-2-nanometer carbon nanotubes. Science 312(5776):1034–1037
39. Kannam SK, Todd BD et al (2013) How fast does water flow in carbon nanotubes? J Chem Phys 138(9):094701

40. Sun L, Huang H et al (2013) Laminar MoS_2 membranes for molecule separation. Chem Commun 49(91):10718–10720
41. Mi B (2014) Graphene oxide membranes for ionic and molecular sieving. Science 343(6172):740–742
42. Walther JH, Ritos K et al (2013) Barriers to superfast water transport in carbon nanotube membranes. Nano Lett 13(5):1910–1914
43. Skoulidas AI, Sholl DS (2002) Transport diffusivities of CH_4, CF_4, He, Ne, Ar, Xe, and SF_6 in silicalite from atomistic simulations. J Phys Chem B 106(19):5058–5067
44. Skoulidas AI, Ackerman DM et al (2002) Rapid transport of gases in carbon nanotubes. Phys Rev Lett 89(18):185901
45. Tansel B, Sager J et al (2006) Significance of hydrated radius and hydration shells on ionic permeability during nanofiltration in dead end and cross flow modes. Sep Purif Technol 51(1):40–47
46. Raidongia K, Huang J (2012) Nanofluidic ion transport through reconstructed layered materials. J Am Chem Soc 134(40):16528–16531
47. Hu S, Lozada-Hidalgo M et al (2014) Proton transport through one-atom-thick crystals. Nature 516:227–230
48. Xu Z (2013) Mechanics of metal-catecholate complexes: the roles of coordination state and metal types. Sci Rep 3:2914
49. Li H, Song Z et al (2013) Ultrathin, molecular-sieving graphene oxide membranes for selective hydrogen separation. Science 342(6154):95–98
50. Kim D, Kim DW et al (2014) Intercalation of gas molecules in graphene oxide interlayer: the role of water. J Phy Chem C 118(20):11142–11148
51. Duan C, Majumdar A (2010) Anomalous ion transport in 2-nm hydrophilic nanochannels. Nat Nanotechnol 5(12):848–852
52. Siria A, Poncharal P et al (2013) Giant osmotic energy conversion measured in a single transmembrane boron nitride nanotube. Nature 494(7438):455–458
53. Talyzin AV, Solozhenko VL et al (2008) Colossal pressure-induced lattice expansion of graphite oxide in the presence of water. Angew Chem Int Ed 47(43):8268–8271
54. Huang H, Mao Y et al (2013) Salt concentration, pH and pressure controlled separation of small molecules through lamellar graphene oxide membranes. Chem Commun 49(53):5963–5965
55. Paci JT, Belytschko T et al (2007) Computational studies of the structure, behavior upon heating, and mechanical properties of graphite oxide. J Phy Chem C 111(49):18099–18111
56. Suk JW, Piner RD et al (2010) Mechanical properties of monolayer graphene oxide. ACS Nano 4(11):6557–6564
57. Song Z, Xu Z et al (2013) On the fracture of supported graphene under pressure. J Appl Mech 80(4):040911
58. Gao W, Majumder M et al (2011) Engineered graphite oxide materials for application in water purification. ACS Appl Mater Interf 3(6):1821–1826
59. Liu H, Wang H et al (2014) Facile fabrication of freestanding ultrathin reduced graphene oxide membranes for water purification. Adv Mater 27(2):249–54
60. Lin S, Buehler MJ (2013) Mechanics and molecular filtration performance of graphyne nanoweb membranes for selective water purification. Nanoscale 5(23):11801–11807
61. Xue M, Qiu H et al (2013) Exceptionally fast water desalination at complete salt rejection by pristine graphyne monolayers. Nanotechnology 24(50):505720
62. Zhu C, Li H et al (2013) Quantized water transport: ideal desalination through graphyne-4 membrane. Sci Rep 3:3163
63. Kou J, Zhou X et al (2014) Graphyne as the membrane for water desalination. Nanoscale 6(3):1865–1870
64. Yin J, Li X et al (2014) Generating electricity by moving a droplet of ionic liquid along graphene. Nat Nanotechnol 9(5):378–383
65. Alberts B, Johnson A et al (2002) Molecular biology of the cell. Taylor & Francis, New York
66. Loh KP, Bao Q et al (2010) Graphene oxide as a chemically tunable platform for optical applications. Nat Chem 2(12):1015